NJC

Accepted Manuscript

This is an *Accepted Manuscript*, which has been through the Royal Society of Chemistry peer review process and has been accepted for publication.

Accepted Manuscripts are published online shortly after acceptance, before technical editing, formatting and proof reading. Using this free service, authors can make their results available to the community, in citable form, before we publish the edited article. We will replace this *Accepted Manuscript* with the edited and formatted *Advance Article* as soon as it is available.

You can find more information about *Accepted Manuscripts* in the Information for Authors.

Please note that technical editing may introduce minor changes to the text and/or graphics, which may alter content. The journal's standard Terms & Conditions and the Ethical guidelines still apply. In no event shall the Royal Society of Chemistry be held responsible for any errors or omissions in this *Accepted Manuscript* or any consequences arising from the use of any information it contains.

ROYAL SOCIETY OF CHEMISTRY

www.rsc.org/njc

Journal Name

ARTICLE

Rapid, morphology-controllable synthesis of GdOF:Ln^{3+} (Ln = Eu, Tb) crystals with multicolor-tunable luminescence properties

Received 00th January 20xx,
Accepted 00th January 20xx

DOI: 10.1039/x0xx00000x

www.rsc.org/

Ruiqing Li, Hailong Xiong, Yimai Liang, Yali Liu, Nannan Zhang and Shucai Gan*

In this paper, GdOF crystals with high uniformity monodispersity and a variety of well-defined morphologies, such as spheres, nanorods, and nanorod bundles have been successfully synthesized via the urea based homogeneous precipitation method followed by a heat treatment. The influence of pH values, fluoride sources and reaction time on the sizes and morphologies was systematically investigated and discussed. The possible formation mechanism for the precursor has been presented. Under ultraviolet excitation, the GdOF:Ln^{3+} (Ln = Eu, Tb) submicron spheres show their characteristic f–f emissions and give red, and green emission, respectively. Moreover, for Tb^{3+}/Eu^{3+} co-doped GdOF phosphors, tunable emissions have been obtained and the color tones can be tuned from green, through yellow, and then to red by simply adjusting the doping Eu^{3+} concentrations. This merit of multicolor emissions in the visible region makes these materials hold great promise for applications in field-emission displays.

1 Introduction

In recent years, lanthanide-doped (Ln^{3+}) doped luminescent materials have aroused fast growing interest because of their applications in various fields, such as drug delivery, field emission displays (FEDs) and white light-emitting diodes (WLEDs) due to their fascinating optical characteristics arising from the intra 4f transitions.[1–4] Till now, it is generally accepted that the morphology and dimensionality of the materials all play important roles in the electronic, optical, magnetic, chemical, and other physical properties. Hitherto, extensive efforts have been devoted to developing effective synthetic strategies to synthesize a variety of luminescent materials with controllable dimensions and shapes.[5–8] However, manipulating the shape of materials is not a straightforward task due to the difficulties involved in controlling the nucleation and complex phenomena of crystal growth during the reaction process. Particularly, the use of shape-control agents during the crystallization process is a typical and efficient strategy to control the morphology and size, in which the functional groups of the agents can preferentially adsorb on the crystal facet and modulate the kinetics of the crystal growth.[9–11] However, the obtained samples always suffer from the unavoidable surface contamination due to the residual organic surfactant, which would affect the physical and chemical properties of the final products.[12,13] Thus, it is challenging to establish an efficient method to synthesize size and morphology controlled luminescent materials by simple, green, economic and mass production processes.

Lanthanide oxyfluorides (LnOFs) have been considered as excellent luminescent host materials due to their high ionicity, low phonon energy, high chemical and thermal stability.[14–17] Among them, GdOF is a promising host matrix for up-conversion and down-conversion luminescence. Therefore, GdOF crystals with different morphologies have been synthesized via several routes, such as hydrothermal, sol–gel method, and precipitation method.[18–20] However, these approaches suffer from drawbacks such as large crystallites, harsh reaction conditions, high environment loads and complicated processes, which severely hamper their potential application.

Herein, we present a controlled synthesis of monodisperse GdOF nano/microcrystals with a variety of well-defined morphologies via the urea based homogeneous precipitation method followed by a heat-treatment process. The effects of various reaction conditions (fluoride sources, and reaction time) on the morphology of the GdOF samples have been discussed in detail. In addition, a systematic study on the photoluminescence (PL) properties of GdOF:Ln^{3+} (Ln = Eu, Tb, Tb/Eu) phosphors have been carried out in detail.

2 Experimental Section

2.1 Materials

The rare-earth oxides Ln_2O_3 (99.99%) (Ln = Y, Eu) and Tb_4O_7 (99.99%) were purchased from the Science and Technology Parent Company of Changchun Institute of Applied Chemistry. $Ln(NO_3)_3$ were prepared by dissolving corresponding metal oxide in dilute HNO_3 solution at elevated temperature with agitation. Other chemicals were purchased from Beijing Chemical Co. All chemicals were of analytical grade and were used directly without further purification.

2.2 Synthesis

In a typical procedure, 1 mmol $Gd(NO_3)_3$ was added to 100 mL aqueous solution containing a certain quantity of urea and 0.25 mmol of $NaBF_4$ at room temperature. Then, dilute $NH_3 \cdot H_2O$ was introduced rapidly into the vigorously stirred solution until pH = 6 and then the beaker was wrapped with polyethylene film. After magnetic stirring for 10 min, the mixture was heated to 90 °C for 3 h in the water bath. The resulting white precipitates were collected by centrifugation, washed several times with deionized water and ethanol, and finally dried at 70 °C in air for 12 h. The final GdOF

* College of Chemistry, Jilin University, Changchun 130026, PR China
E-mail: gansc@jlu.edu.cn

product was obtained by a heat treatment of the precursors at 500 °C in air for 2 h. Other samples were prepared by a similar procedure, except for different F^- sources, pH conditions and reaction time. The doped GdOF samples were prepared in a similar approach by introducing the proper amounts of $Ln(NO_3)_3$ instead of $Gd(NO_3)_3$ to the solution as described above.

2.3 Characterization

The samples were examined by powder X-ray diffraction (XRD) measurements performed on a Rigaku D/max-II B X-ray diffractometer at a scanning rate of 10°/min in the 2θ range from 10° to 80°, with graphite-monochromatic Cu K_α radiation (λ = 0.15406 nm). Fourier transform infrared (FT-IR) spectra were recorded on a Perkin-Elmer 580B infrared spectrophotometer using the KBr pellet technique. The morphology, dimensions, and composition of the as-synthesized nano-/microstructures were examined by means of scanning electron microscopy (SEM, S-4800, Hitachi) equipped with an energy-dispersive X-ray spectrum (EDX, JEOL JXA-840). The photoluminescence excitation and emission spectra were recorded with a Hitachi F-7000 spectrophotometer equipped with a 150W xenon lamp as the excitation source. The luminescence decay curves were obtained using a FLS920 (Edinburgh Instrument). All measurements were performed at room temperature.

3 Results and discussion

3.1 Phase identification, and morphology

The composition and phase purity of the samples were first examined using XRD. Fig. 1a shows the XRD patterns of the as-prepared GdOF precursor using $NaBF_4$ as the F^- source, the annealed sample, and the standard data of GdOF, respectively. No obvious diffraction peaks can be observed from the precursor sample, which indicates that the sample is amorphous. After calcining at 500 °C for 2h, it can be seen that well-defined diffraction peaks can be assigned readily to the rhombohedral phase of GdOF (JCPDS no.

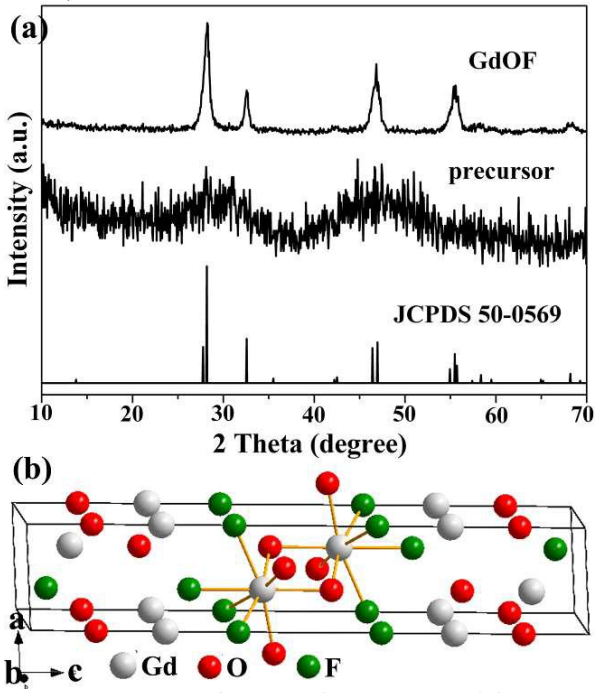

Fig. 1 (a) XRD patterns of as-prepared precursor, annealed at 500 °C samples, and the standard data of GdOF (JCPDS no. 05–0569). (b) Schemes of the tetragonal phase GdOF structures.

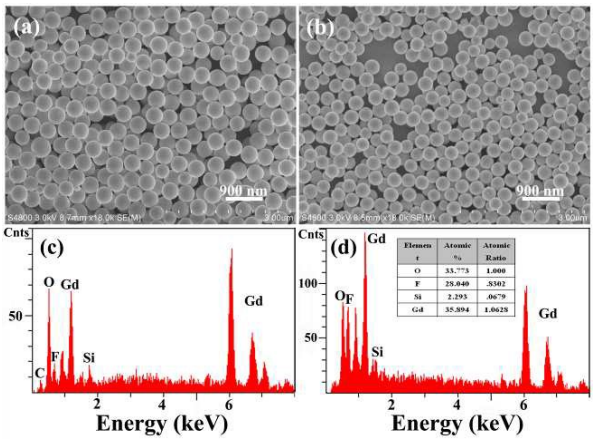

Fig. 2 SEM images of the as-prepared precursor sample (a) and GdOF obtained by calcining the precursor at 500 °C (b). EDX spectra of as-prepared precursor sample (c) and GdOF obtained by calcining the precursor at 500 °C (d). The inset shows the quantificational ratio of the elements calculated from EDX data.

50–0569), and no peak shifts and other impurity phases appear, revealing the high purity and crystallinity of the product. Fig. 1b shows its schematic view of the structure and coordination environments. The Gd^{3+} cations are coordinated by four O^{2-} and four F^-, and all ions occupy the six-fold 6c Wyckoff positions with the same C_{3v} site symmetry.[21]

The SEM and EDX spectra images of the precursor and GdOF sample prepared at pH = 6 with $NaBF_4$ as the F^- source are shown in Fig. 2. It is obvious that the precursor composed of a great number of highly monodispersed spheres with average diameter about 420 nm and the surfaces are smooth, as displayed in Fig. 2a. The SEM image shown in Fig. 2b reveals that GdOF still retains the spheres morphology, but their size (diameter about 350 nm) was slightly shrunk and the surfaces became rough due to the decomposition of the precursor and crystallization of GdOF, during the subsequent calcination process. EDX spectra confirm the presence of Gd, C, O and F elements from the precursor samples (Fig. 2c). After calcinations, the element C almost disappeared (Si from the Si substrate), and the samples mainly consists of Gd, O and F (Fig. 2d). the atomic ratio of the sample (Gd:O:F = 1.06:1:0.83) can be calculated, which is in agreement with the stoichiometric atomic ratio of the GdOF sample.

Control experiments demonstrated that fluoride sources and pH values play dominant roles in adjusting the morphologies and sizes of GdOF in the following paragraphs. The SEM images of GdOF using NaF, NH_4F, NH_4BF_4 and NH_4HF_2 as the fluorine ion sources are shown in Fig. 3, respectively. Different from the nanospheres using NaF and as a fluorine sources, the obtained sample (Fig. 3a) is composed of monodispersed nanorods with length about 1.72 μm and diamete about 76 nm and these nanorods have rough surfaces.When using NH_4F as a fluorine source, the as-obtained product comprises of a large quantity of nanorods (a length of about 1.9 μm, a diameter of about 115 nm), as shown in Fig. 3b. When NH_4BF_4 was used as the F^- source, monodispersed microspheres with diameter about 2 μm were obtained, as shown in Fig. 3c. For the NH_4HF_2 (Fig. 3d) system, it can be seen that the obtained samples are composed of monodispersed nanospindles and nanorod bundles. Therefore, the above results show that the different F^- sources have a tremendous effect on the morphologies and sizes of the products. In our system, the cations of Na^+, NH_4^+ and H^+ ions could be selectively adsorbed on different surfaces of initial precursor crystals due to the strong interactions between these cations and OH^-, CO_3^{2-}, and F^- anions during the early stage of the

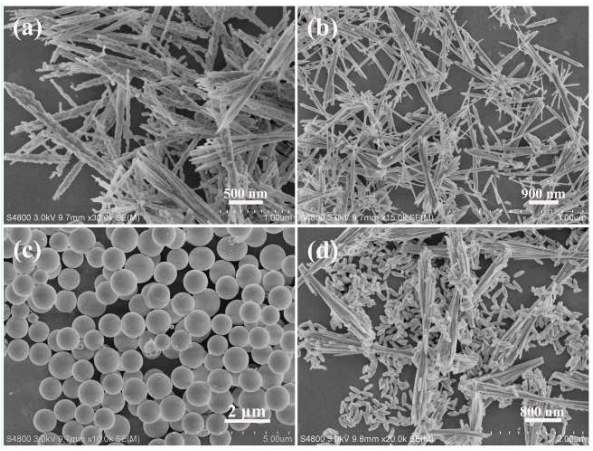

Fig. 3 SEM images of the GdOF samples prepared at pH = 6 with NaF (a), NH_4F (b), NH_4BF_4 (c), and NH_4HF_2 (d).

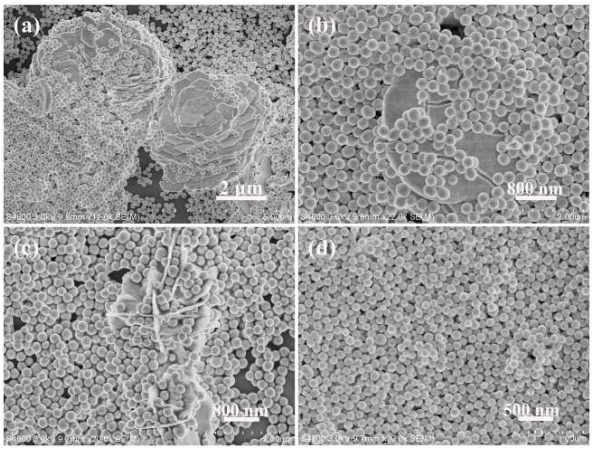

Fig. 4 SEM images of the synthesized samples with the pH values of the initial solution at pH = 2 (a), pH = 3 (b), pH = 4 (c), and pH = 5 (d).

reactions and influence the corresponding surface energy, thus leading to the various morphologies.[22,23]

Fig. 4 shows the SEM images of the products obtained under the same conditions but various pH values. As seen from the SEM images, GdOF materials can be obtained by simply adjusting the pH values of the initial solution. At pH = 2, the obtained GdOF crystals consist of large quantity of uniform nanospheres and few bulk particles (Fig. 4a). When the pH further increases to 3, the size of the bulk particles decreases (Fig. 4b). By increasing the pH from 3 to 4 (Fig. 4c), the bulk particles turn into assembled nanosheets. Close observation reveals that many nanospheres attach to the surface of nanosheets. As the pH increased to 5, the products consist of nanospheres with diameters of about 140 nm (Fig. 4d). This result indicates that changing the pH values of the initial solution have important influence on the morphology of the final products. As we know, the hydrolysis of $NaBF_4$ produces many dissociated F^- ions: $BF_4^- + 3H_2O \rightarrow 3HF + F^- + H_3BO_3$ in aqueous solution.[24] The release of F^- is favorable when the pH is high and higher pH point to a higher concentration of F^- in the solution. When temperature is above 83 °C, the urea decomposition to produce the precipitating ligands (mainly OH^- and CO_3^{2-}).[25,26] An increasing pH value would generate high concentration of F^- and accelerate the precipitation of Gd^{3+} to some extent, thus decreasing the concentration of Gd^{3+} and eventually affecting the facets' growth kinetics.[27] In conclusion, the above results prove that our approach is environmentally benign

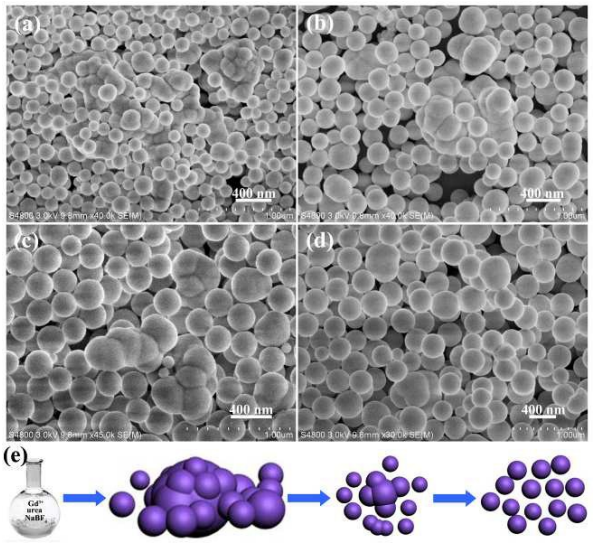

Fig. 5 SEM images of as-prepared precursor samples for different reaction times: 10 min (a), 20min (b), 30 min (c) and 1 h (d) using $NaBF_4$ as the F^- source. Schematic diagram of the formation process of YOF submicro spheres (e).

without adding any chelating agents or organic solvents and efficient to prepare morphologies controlled nano/microscale luminescent materials.

To understand the growth mechanism of the GdOF spheres, time-dependent experiments were carried out by keeping other reaction parameters unchanged (90 °C, pH = 6 with $NaBF_4$ as F^- source), which is presented in Fig. 5. At 10 min, the OH^- and CO_3^{2-} were released from the decomposition of urea at high temperature in aqueous solution. Subsequently, a fast nucleation process occurred and a large number of spheres and irregular bulk particles can be obtained, as shown in Fig. 5a. Close observation reveals that many spheres formed on the surface of bulk particles. When the reaction time is increased to 20 min (Fig. 5b), the size of bulk particles is decreasing and generating more spheres in order to reduce the energy of the reaction system. At a reaction time of 30 min (Fig. 5c), the size of bulk particles is further decreasing. When the reaction time is prolonged to 1 h (Fig. 5d), the bulk particles almost dissolve and the size uniformity is greatly improved. With further growth, the uniform nanospheres are obtained. On the basis of the time-dependent results and analysis, we hypothesize that the conversion process from amorphous bulk particles to spheres can be rationally expressed as a dissolution–recrystallization mechanism and a schematic illustration for the formation of the GdOF product is presented in Fig. 5e.

3.2 Luminescence properties

Eu^{3+} ion is a well-known red-emitting activator in commercial phosphors because the emission of the rare earth Eu^{3+} ion consists usually of lines in the red spectral area due to the $^5D_0 \rightarrow {}^7F_J$ (J = 1, 2, 3, 4, 5 and 6) transitions. While the Tb^{3+} ion is used as an activator in green phosphors, whose emission is mainly due to the transitions of $^5D_3 \rightarrow {}^7F_J$ in the blue region and $^5D_4 \rightarrow {}^7F_J$ in the green region (J = 6, 5, 4, 3, 2), depending on its doping concentration. Fig. 6 shows the PL excitation and emission spectra of GdOF:0.03Eu^{3+} and GdOF:0.03Tb^{3+} samples, respectively. The PL excitation spectrum of GdOF:0.03Eu^{3+} (Fig. 6a) shows a strong band with a maximum at 254 nm, which is ascribed to the charge transfer band (CTB) between the O^{2-} and Eu^{3+} ions. The excitation peaks at 311 nm originated from the transitions of $^8S_{7/2} \rightarrow {}^6P_{7/2}$ of the Gd^{3+}.[28] In addition, the weaker lines in the long wavelength regions of 320–500

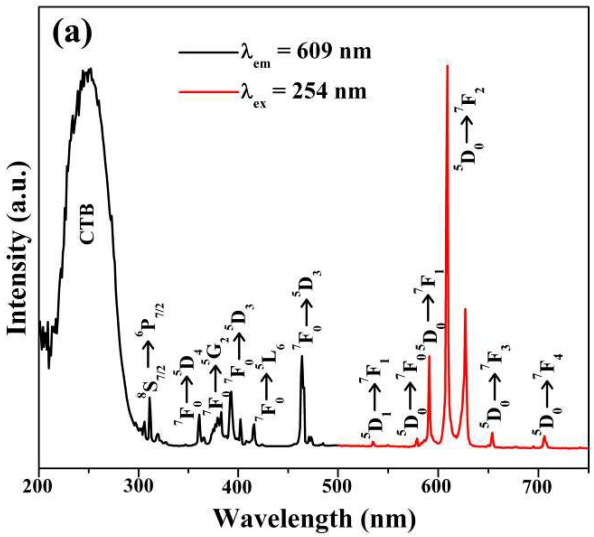

Fig. 6 PL excitation and emission spectra of the GdOF:0.03Eu^{3+} (a), and GdOF:0.03Tb^{3+} phosphors (b).

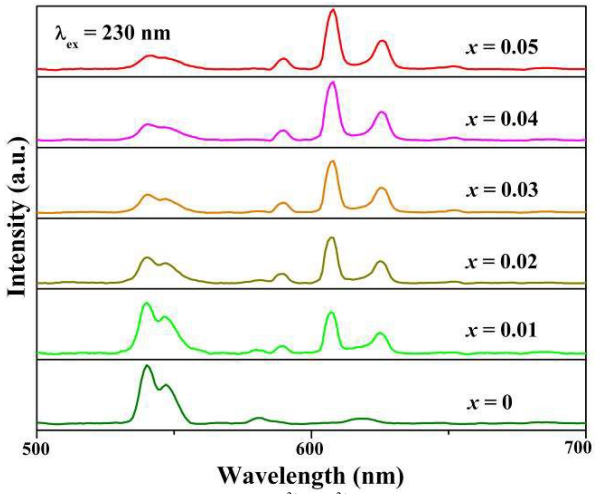

Fig. 7 PL spectra for GdOF:0.03Tb^{3+},$x$$Eu^{3+}$ phosphors as a function of the Eu^{3+} doping content (x).

nm are assigned to the f–f intra-configuration transitions of the Eu^{3+} ions.[29] Upon excitation at 254 nm, the GdOF:0.03Eu^{3+} phosphor shows a strong red emission with the CIE (Commission Internationale de l'Eclairage 1931 chromaticity) chromaticity coordinate (0.660,0.341) (point a in Fig. 8). The emission spectrum consists of the characteristic transitions at 535 nm, 578 nm, 591 nm, 609 nm, 627 nm, 654 nm and 704 nm, which are assigned to the $^5D_1 \rightarrow {}^7F_1$ and $^5D_0 \rightarrow {}^7F_J$ (J = 0, 1, 2, 3, 4) transitions of Eu^{3+}, respectively.[30] Obviously, the emission spectrum is dominated by the hypersensitive red transition ($^5D_0 \rightarrow {}^7F_2$) of Eu^{3+}, indicating that the Eu^{3+} ions are located at sites without or deviating from inversion symmetry.[31] The excitation spectrum of GdOF:0.03Tb^{3+} (Fig. 6b) mainly consists of strong absorption at 203 nm and 230 nm which are ascribed to the host absorption and spin-allowed transition (ΔS = 0) with high energy from the 4f to 5d of the Tb^{3+} ions, respectively.[32] Under 230 nm UV radiation excitation, the as-prepared GdOF:0.03Tb^{3+} is composed of a group of lines centered at about 491 nm, 540 nm, 581 nm, and 619 nm, which correspond to the $^5D_4 \rightarrow {}^7F_J$ (J = 6, 5, 4, 3) transitions of the Tb^{3+} ions, respectively.[33] The CIE coordinate for the emission spectrum of GdOF:0.03Tb^{3+} is determined as (0.275, 0.643), located in the green region.

It has been reported that a wide-range-tunable light emission were obtained by precise control of the contents of Eu^{3+} and Tb^{3+} ions in host.[34,35] In order to obtain the multicolor tunable luminescence, the Tb^{3+}, Eu^{3+} ions co-doped GdOF samples were synthesized in our work. Fig. 7 shows the emission spectra of the Eu^{3+} and Tb^{3+} co-doped GdOF samples under excitation at 230 nm. It can be seen that the as-obtained purely Tb^{3+} doped GdOF sample depicts strong green emission under excitation with UV light. By co-doping the GdOF host lattice with Eu^{3+} and Tb^{3+} ions, the characteristic emission of both Tb^{3+} and Eu^{3+} are observed. Furthermore, with increasing the Eu^{3+} concentration, the emission intensities of the Tb^{3+} ion decreases monotonically whereas the emission intensities of Eu^{3+} gradually increases under 230 nm UV radiation excitation.

To further validate the energy transfer from Tb^{3+} to Eu^{3+}, the decay curves of Tb^{3+} in GdOF:0.03Tb^{3+}, $x$$Eu^{3+}$ (x = 0-0.05) phosphors excited at 230 nm and monitored at 540 nm were measured and depicted in Fig. 6. It was found that the luminescent decay curves can be well fitted with a single exponential decay mode as the following equation:[36]

$$I(t) = I_0 \exp(-t/\tau)$$

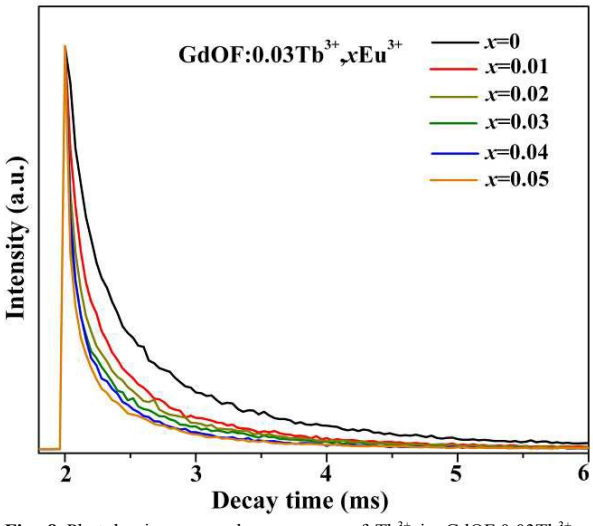

Fig. 8 Photoluminescence decay curves of Tb^{3+} in GdOF:0.03Tb^{3+}, $x$$Eu^{3+}$ phosphor (excited at 230 nm, monitored at 540 nm).

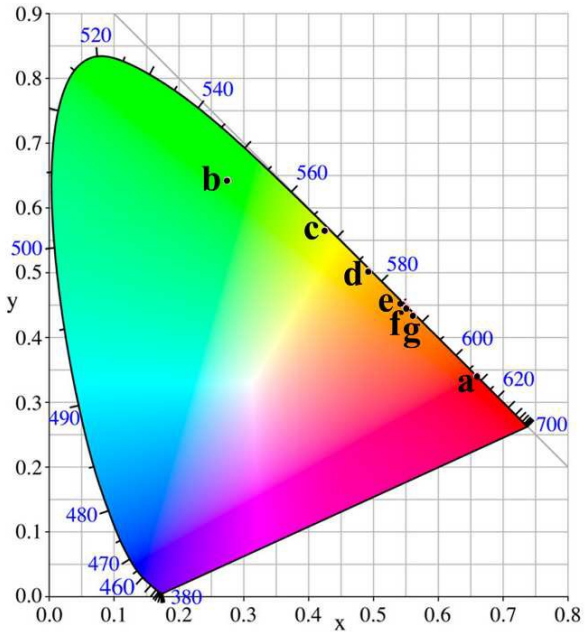

Fig. 9 The CIE chromaticity diagram of the GdOF:0.03Eu^{3+} and GdOF:0.03Tb^{3+},xEu^{3+} (x = 0, 0.01, 0.02, 0.03, 0.04, 0.05) phosphors.

Table 1 The CIE chromaticity coordinates (x, y) for the GdOF:0.03Eu^{3+} and GdOF:0.03Tb^{3+},xEu^{3+} samples upon excitation at 230 nm

Sample no.	Sample compositions	CIE (x, y)	CCT (K)
a	GdOF:0.03Eu^{3+}	(0.660, 0.341)	2973
b	GdOF:0.03Tb^{3+}	(0.275, 0.643)	6427
c	GdOF:0.03Tb^{3+}, 0.01Eu^{3+}	(0.429, 0.565)	3988
d	GdOF:0.03Tb^{3+}, 0.02Eu^{3+}	(0.492, 0.503)	2914
e	GdOF:0.03Tb^{3+}, 0.03 Eu^{3+}	(0.546, 0.452)	2099
f	GdOF:0.03Tb^{3+}, 0.04 Eu^{3+}	(0.550, 0.447)	2042
g	GdOF:0.03Tb^{3+}, 0.05Eu^{3+}	(0.562, 0.435)	1906

where $I(t)$ and I_0 are the luminescence intensities at time t and 0, and τ is the radiative decay time. On the basis of the equation, the effective lifetime values were calculated to be 4.09, 2.71, 2.29, 2.02, 1.84, and 1.57 ms for GdOF:0.03Tb^{3+}, xEu^{3+} with x = 0, 0.01, 0.02, 0.03, 0.04, and 0.05, respectively, which confirms the efficient energy transfer from Tb^{3+} to Eu^{3+} ions.

Fig. 9 shows the CIE chromaticity diagram for the emission spectra of GdOF:0.03Eu^{3+} and GdOF:0.03Tb^{3+},xEu^{3+}as a function of the Eu^{3+} doping concentration. It can be clearly seen that the color hue of samples change from green, through yellow and finally to red by simply adjusting the relative doping concentrations of the Eu^{3+}. The correlated color temperature (CCT) as one of the characteristics of samples has also been obtained and the results are presented in Table 1. These results show that the as-obtained phosphors with multicolor emissions might find potential applications in FEDs.

4 Conclusion

In summary, multiform GdOF structures, including spheres, nanorod, and nanorod bundles have been synthesized via a facile modified urea based homogeneous precipitation method followed by a heat treatment. The influences of pH values and fluoride sources on the morphologies of GdOF have been investigated in detail. The possible formation mechanism for the precursor has been presented based on time-dependent experiments. Moreover, various luminescence colors could be obtained easily in GdOF:Ln^{3+} spheres because of the characteristic f−f transitions under UV light excitation. The emission color of obtained phosphors can be varied from green to red by adjusting the concentration of Eu^{3+}. These results indicate that GdOF:Tb^{3+},Eu^{3+} can be promising as a potential candidate for the application in white FEDs.

Acknowledgements

This present work was financially supported by Practical Research (MORCUATPPR) funded by China Geological Survey (Grant No. 12120113088300).

References

1 J. N. Liu, W .B. Bu, L. M. Pan, and J. L. Shi, *Angew. Chem. Int. Ed.*, 2013, **52**, 4375.
2 G. Tian, Z. J. Gu, L. J. Zhou, W. Y. Yin, X. X. Liu, L. Yan, S. Jin, W. L. Ren, G. Xing, S. Li, and Y. L. Zhao, *Adv. Mater.*, 2012, **24**, 1226.
3 G. Zhu, Z. P. Ci, Q. Wang, Y. Wen, S. C. Han, Y. R. Shi, S. Y. Xin and Y. H. Wang, *J. Mater. Chem. C*, 2013, **1**, 4490.
4 X. F. Li, J. D. Budai, F. Liu, J. Y. Howe, J. Zhang, X. J. Wang, Z. Gu, C. Sun, R. S. Meltzer and Z. W. Pan, *Light Sci. Appl.*, 2013, **2**, e50.
5 G. Jia, H. P. You, K. Liu, Y. Zheng, N. Guo, J. Jia, and H. J. Zhang, *Chem. Eur. J.*, 2010, **16**, 2930.
6 Z. Xu, C. X. Li, D. Yang, W. Wang, X. J. Kang, M. Shang and J. Lin, *Phys. Chem. Chem. Phys.*, 2010, **12**, 11315.
7 S. Huang, J. Xu, Z. Zhang, X. Zhang, L. Wang, S. L. Gai, F. He, N. Niu, M. Zhang and P. P. Yang, *J. Mater. Chem.*, 2012, **22**, 16136.
8 R. Q. Li, L. L. Li, Y. M. Liang, N. N. Zhang, Y. L. Liu and S. C. Gan, *Phys. Chem. Chem. Phys.*, 2015, **17**, 21485
9 L. Xu, C. Lu, Z. Zhang, X. Yang and W.H. Hou, Nanoscale, 2010, 2, 995.
10 Y. Zhang , Z. Wu , D. L. Geng, X. Kang , M. M. Shang, X. Li , H. Z. Lian , Z. Y. Cheng , and J. Lin, *Adv. Funct. Mater.*, 2014, **24**, 6581.
11 Y. Wang, S. L. Gai, N. Niu, F. He and P. P. Yang, *Phys. Chem. Chem. Phys.*, 2013, 15, 16795.
12 S. Mourdikoudis and L. M. Liz-Marzán, *Chem. Mater.*, 2013, 25, 1465.
13 C. C. Yang, Y. H. Yu, B. Linden, J. C. Wu and G. Mul, *J. Am. Chem. Soc.*, 2010, **132**, 8398.
14 Y. Zhang, X. J. Li, Z. Y. Hou and J. Lin, *Nanoscale*, 2014, **6**, 6763.
15 G. Q. Chai, G. P. Dong, J. R. Qiu, Q. Y. Zhang, Z. M. Yang, *Sci. Rep.*, 2013, **3**, 1598.
16 R. Q. Li, N. N. Zhang, L. L. Li, Y. M. Liang, Y. L. Liu and S. C. Gan, *New J. Chem.*, 2015, **39**, 7019.
17 N. Rakov, S.A. Vieira, R. B. Guimarães, G. S. Maciel, *J. Alloys Compd.*, 2015, **618**, 127.
18 L. Tao, W. Xu, Y. S. Zhu, L. Xu, H. Zhu, Y. X. Liu, S. Xu, P. P. Zhou and H. W. Song, *J. Mater. Chem. C*, 2014, **2**, 4186.
19 Y. Zhang, X. Kang, D. L. Geng, M. M. Shang, Y. Wu, X. Li, H. Z. Lian, Z. Y. Cheng and J. Lin, *Dalton Trans.*, 2013, **42**, 14140.
20 T. Passuello, F. Piccinelli, M. Pedroni, S. Polizzi, F. Mangiarini, F. Vetrone, M. Bettinelli, A. Speghini, *Opt. Mater.*, 2011, **33**, 1500.
21 T. Grzyb, M. Wcławiak, S. Lis, *J. Alloys Compd.*, 2012, **539**, 82.

22 L. Vayssieres, C. Chaneac, E. Tronc, and J. P. Jolivet, *J. Colloid Interf. Sci.*, 1998, **205**, 205.
23 M. Wang, Q. L. Huang, J. M. Hong, X. T. Chen, and Z. L. Xue, *Cryst. Growth Des.*, 2006, **6**, 2169.
24 Q. Zhao, B. Q. Shao, W. Lü, W. Z. Lv, M. M. Jiao, L. F. Zhao, and H. P. You, *Dalton Trans.*, 2015, **44**, 3745.
25 R. Q. Li, G. H. Yu, Y. M. Liang, N. N. Zhang, Y. L. Liu, S. C. Gan, *J. Colloid Interf. Sci.*, 2015, **460**, 273.
26 J. G. Li, X. D. Li, X. D. Sun, T. Ikegami, and T. Ishigaki, *Chem. Mater.*, 2008, **20**, 2274.
27 Y. Zhang, D. L. Geng, X. J. Kang, M. M. Shang, Y. Wu, X. J. Li, H. Z. Lian, Z. Y. Cheng, and J. Lin, *Inorg. Chem.*, 2013, **52**, 12986.
28 M. L. Debasu, D. Ananias, J. Rocha, O. L. Maltac and L. D. Carlos, *Phys. Chem. Chem. Phys.*, 2013, **15**, 15565.
29 S. K. Gupta, S. Nigam, A. K. Yadav, M. Mohapatra, S. N. Jha, C. Majumder and D. Bhattacharyya, *New J. Chem.*, 2015, **39**, 6531.
30 R. Q. Li, W. W. Zi, L. L. Li, L. Liu, J. J. Zhang, L. C. Zou, S. C. Gan, *J. Alloys Compd.*, 2014, **617**, 498.
31 W. X. Wang, Z. Y. Cheng, P. P. Yang, Z. Y. Hou, C. X. Li, G. G. Li , Y. L. Dai, and J. Lin, *Adv. Funct. Mater.*, 2011, **21**, 456.
32 C. Peng, M. M. Shang, G. G. Li, Z. Y. Hou, D. L. Geng, and J. Lin, *Dalton Trans.*, 2012, **41**, 4780.
33 A. Watras, P. J. Dereń and R. Pazik, *New J. Chem.*, 2014, **38**, 5058.
34 R. Li, Y. L. Liu, N. Zhang, L. Li, L. Liu, Y. M. Liang and S. Gan, *J. Mater. Chem. C*, 2015, **3**, 3928.
35 Z. Y. Hou, Z. Y. Cheng, G. G. Li, W. X. Wang, C. Peng, C. X. Li, P. Ma, D. M. Yang, X. J. Kang and J. Lin, *Nanoscale*, 2011, **3**, 1568.
36 L. Zhang, L. L. Fu, X. X. Yang, Z. L. Fu, X. D. Qi and Z. J. Wu, *J. Mater. Chem. C*, 2014, **2**, 9149.

Graphical Abstract

This work investigates a facile and mass-production method to synthesize multiform morphologies of GdOF and obtains multicolor emissions in GdOF:Tb^{3+},Eu^{3+} samples.